THE JOURNAL OF PHYSICAL CHEMISTRY C

Article

pubs.acs.org/JPCC

Electronics and Optics of Graphene Nanoflakes: Edge Functionalization and Structural Distortions

Caterina Cocchi,*[,†,‡] Deborah Prezzi,*[,†] Alice Ruini,[†,‡] Marilia J. Caldas,[§] and Elisa Molinari[†,‡]

[†]Centro S3, CNR-Istituto Nanoscienze, I-41125 Modena, Italy

[‡]Dipartimento di Fisica, Università di Modena e Reggio Emilia, I-41125 Modena, Italy

[§]Instituto de Física, Universidade de São Paulo, 05508-900 São Paulo, SP, Brazil

Supporting Information

ABSTRACT: The effects of edge covalent functionalization on the structural, electronic, and optical properties of elongated armchair graphene nanoflakes (AGNFs) are analyzed in detail for a wide range of terminations, within the framework of Hartree−Fock-based semiempirical methods. The chemical features of the functional groups, their distribution, and the resulting system symmetry are identified as the key factors that determine the modification of strutural and optoelectronic features. While the electronic gap is always reduced in the presence of substituents, functionalization-induced distortions contribute to the observed lowering by about 35−55%. This effect is paired with a red shift of the first optical peak, corresponding to about 75% of the total optical gap reduction. Further, the functionalization pattern and the specific features of the edge−substituent bond are found to influence the strength and the character of the low-energy excitations. All of these effects are discussed for flakes of different widths, representing the three families of AGNFs.

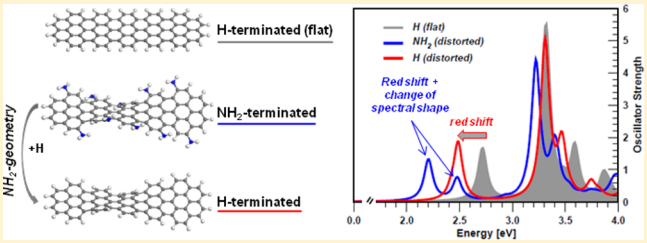

The electronic,[1−4] optical,[5−7] and magnetic properties[8−10] of graphene nanoribbons are closely related to their edge morphology, and indeed, several theoretical proposals have been advanced to tune the properties of these systems through edge modifications. For instance, the termination of edge C atoms with different groups[11−14] and the introduction of magnetic impurities[15−18] at the edges of zigzag graphene nanoribbons represent promising routes to fully exploit their potential for spintronics applications. In armchair graphene nanoribbons (AGNRs), on top of the intrinsic tunability given by the well-established family behavior,[2,3] edge modifications can further engineer the energy gap and work function,[19−23] as well as their optical response.[24−26]

An additional aspect of edge modifications is related to the appearance of structural distortions: ripples and twists can arise, either localized at the edge region[27,28] or extended to the whole structure, with effects on a larger scale.[29−31] Indeed, the study of structural modifications has drawn itself great attention, since they can lead to a further tuning of the graphene nanostructure properties.[32,33] We here focus on unraveling the effects of functionalization-induced structural, electronic, and optical modifications, considering not only the functional group itself but also the functionalization pattern. Such analysis can be particularly relevant to designing new optoelectronic functionalities in graphene nanostructures, above all, in light of the recent improvements in their controlled synthesis at the nanoscale.[34−40]

We carry out our analysis on short armchair graphene ribbons functionalized with different edge substituents, ranging from single atoms to small molecular moieties. Family dependence is also taken into account. We recognize that several factors—including the system symmetry, the chemical features of the functional groups, and their distribution—are responsible for the appearance of different structural and optoelectronic modifications. In general, the steric hindrance of substituents is found to induce local distortions at the edges, but global effects involving the flake backbone can also arise in specific cases. These structural modifications are found to reduce the electronic gap up to 300 meV, corresponding to 55% of the total gap decrease. This effect is associated with a similar red shift of the first optical peak. On the other hand, the chemical features of the substituents and their arrangement at the edges crucially influence the distribution of the frontier orbitals. Local variations arise as a consequence of the modified molecular symmetry upon edge functionalization, while global localization effects are noticed when a large longitudinal dipole component is introduced by polar substituents. Moreover, such a charge redistribution results in the appearance of an additional peak in the low-energy region of the spectra, related to the optical activation of an otherwise dark excitation.

METHODS AND SYSTEM DESCRIPTION

The results presented in this paper are obtained within the framework of Hartree−Fock-based semiempirical methods,[41]

Received: January 19, 2012
Revised: June 11, 2012
Published: July 31, 2012

which are well-tested and reliable for the evaluation of the electronic and optical properties of C-conjugated low-dimensional systems.[42−45] The AM1 model[46] is adopted for structural optimization (0.4 kcal·mol^{-1}/Å threshold for the forces) and for the study of the electronic properties, including the calculation of electric dipole moments. The electronic gap is computed as the difference between the *vertical* ionization potential (IP) and the electron affinity (EA), which are, in turn, obtained from the total energy of the neutral and (±1) charged states, that is, IP = $E(+1) - E(0)$ and EA = $E(0) - E(-1)$. The optical spectra are evaluated by means of the ZINDO/S model,[47] with single excitation configuration interaction (CIS). Our convergence tests over the number of occupied and virtual molecular orbitals (MOs) indicated that a CI energy window of at least 4.5 eV below the HOMO and 3.5 eV above the LUMO is required for a reliable characterization of the low-energy optical excitations.

We perform our analysis on elongated graphene nanoflakes (GNFs) with armchair-shaped edges, which can be seen as finite portions of graphene nanoribbons. As for infinite ribbons, we introduce a width parameter, N, corresponding to the number of dimeric C lines across the y axis (see Figure 1a). According to their width parameter, N, both ribbons[2,3] and flakes[23] present three scaling laws for the energy gap, also in the presence of edge substituents. This allows us to classify them into three different families, following a *modulo* 3 periodic law: $N = 3p + m$, with p integer and $m = 0, 1, 2$. In the following, we will mainly focus on an $N = 7$ GNF (width ∼ 7.3 Å) with a length of ∼24 Å (x axis; see Figure 1a). We will then extend our analysis to the family dependence by considering two additional structures (shown in Figure 1b,c), having widths of 8.6 Å ($N = 8$) and 9.8 Å ($N = 9$) and keeping the length fixed. For each structure, the lateral ends along the x axis are shaped in such a way as to minimize the influence of zigzag edges, which are known to affect the electronic properties of the system.[48,49]

The effects of edge substituents on the electronic and optical properties of GNFs are investigated for a number of light-element metal-free functional groups, including atoms and molecular groups typically involved in electrophilic aromatic substitutions.[50,51] We group these terminations into three main classes, with respect to the nature of their covalent bond with the graphene edge: the first class comprises monovalent halogen terminations (F, Cl, and Br); the second one consists of groups forming a direct bond at the edge, in which either N or O shares a 2p lone pair with the edge C atom (NH_2, OCH_3, and $OCF{=}CF_2$); as a third class, we finally consider small moieties bonded to the GNF through a C bond and including a C double bond, which allows extending the C-conjugation of the graphene backbone for one additional bond length beyond the edge ($COCH_3$, $CH{=}CH_2$, and $CH{=}CF_2$). The choice of these terminations is basically motivated by their experimental feasibility in systems similar to those investigated here.[34,52−54]

Edge covalent functionalization is here performed by replacing each second H atom passivating the armchair edges in the reference system, through the regular alternation of substituents. As indicated in Figure 1, two functionalization schemes can be designed: in the A-A scheme, the same C zigzag line is functionalized on opposite edges, whereas in the A-B scheme, alternating C zigzag lines are functionalized. In addition, full substitution, that is, functionalization of all C edge atoms, is considered for monoatomic halogen terminations only, as justified by their reduced size. Note that,

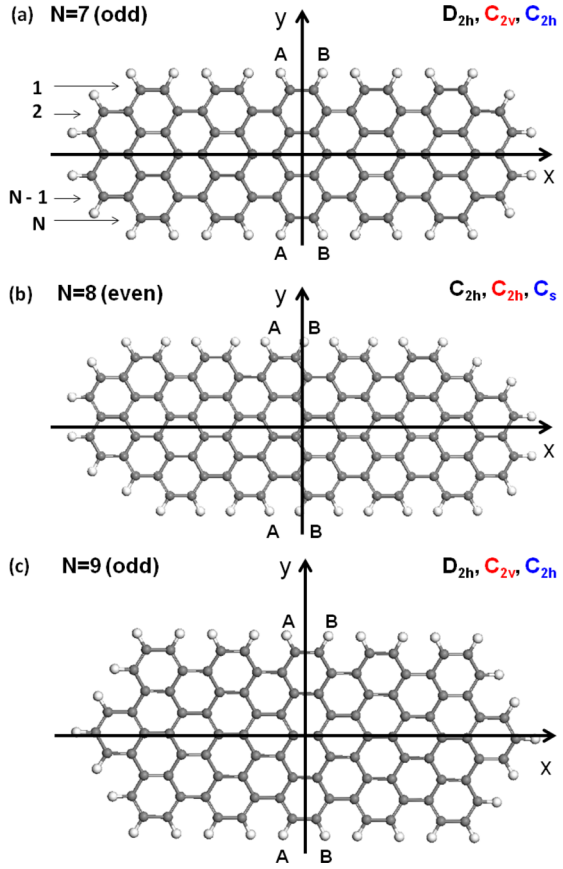

Figure 1. H-terminated armchair graphene nanoflakes (AGNFs) of fixed length (x axis) and variable width (y axis), chosen as representative of the three different families of AGNFs, i.e., $N = 3p$, $3p + 1$, and $3p + 2$. Edge functionalization is performed by replacing each second H atom along the length with a foreign substituent. Two functionalization schemes can be identified: the A-A scheme, where the same zigzag line is functionalized on both edges, and the A-B scheme, where functionalization involves alternating zigzag lines. Indicated are the point symmetry groups of each structure, clean (black) and functionalized in the A-A (red) and A-B (blue) schemes, respectively, for ideal (nondistorted and symmetrically terminated) flakes.

depending on the chosen scheme and on the flake width, each structure has a different symmetry. H-terminated flakes have D_{2h} (C_{2h}) symmetry for odd (even) N, which is modified by the presence of functional groups at the edges. For odd N, the A-A scheme results in a C_{2v} symmetry, whereas in the A-B scheme, the symmetry is C_{2h}. On the contrary, for even N, the symmetry is preserved as C_{2h} in the A-A scheme and lowered to C_s in the A-B scheme. Even though this classification is formally correct only for ideal nondistorted and symmetrically terminated structures, since the symmetry is always lowered upon structural optimization, we will keep this notation throughout the paper for convenience.

RESULTS AND DISCUSSION

Edge covalent functionalization is known to be an effective strategy to tune the electronic gap of graphene nanostructures.[19,20,22,32] As suggested already for simple aromatic compounds,[55−57] the presence of edge functional groups modifies the electronic distribution within the graphene network in the edge proximity. As a consequence, heterospecies with different electronegativities than C and covalently bonded

dx.doi.org/10.1021/jp300657k | J. Phys. Chem. C 2012, 116, 17328−17335

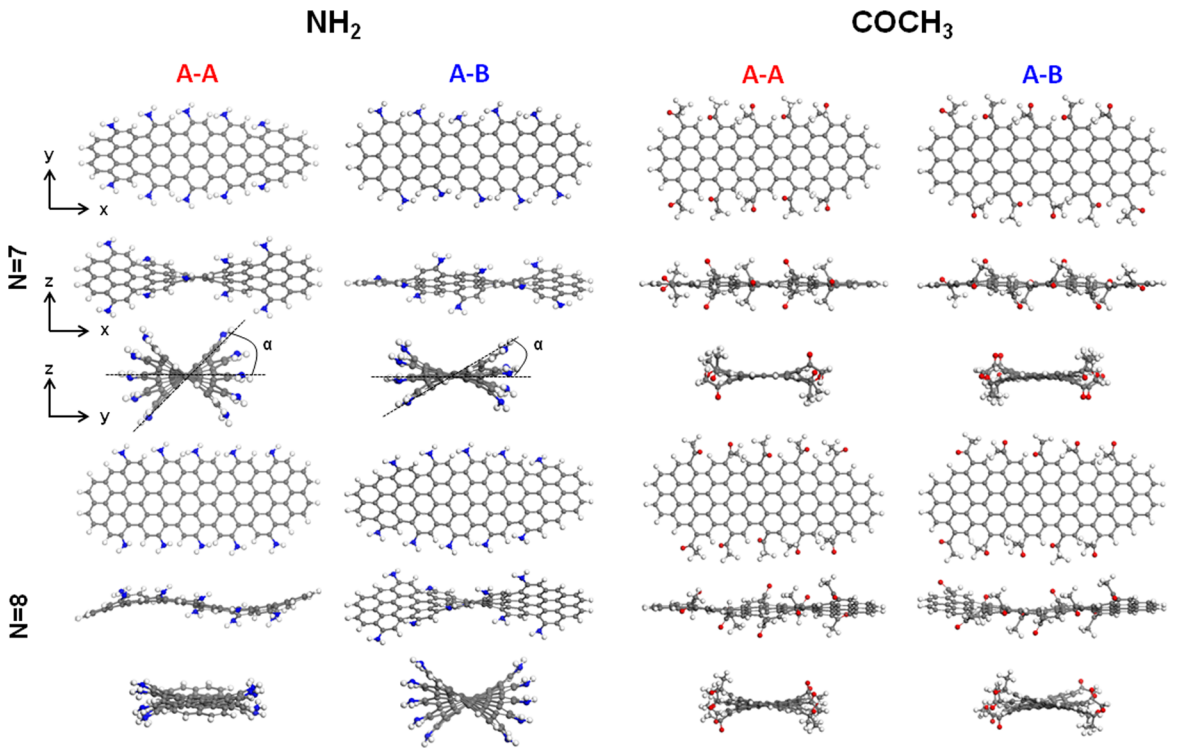

Figure 2. Structurally optimized $N = 7$ and $N = 8$ AGNFs, functionalizalized with NH_2 (left) and $COCH_3$ (right) groups, according to the A-A and A-B schemes. The angle α is introduced to quantify the distortion angle, defined as the maximum deviation from planarity of edge C atoms.

Table 1. Distortion Angles α (in deg) for $N = 7$ GNFs Functionalized According to the Indicated Schemes (1st Column)[a]

	halogen			direct bond			C bond		
	F	Cl	Br	NH_2	OCH_3	$OCF{=}CF_2$	$COCH_3$	$CH{=}CF_2$	$CH{=}CH_2$
A-A	7.2	11.3	12.0	36.5	11.1	22.2	10.5	19.2	25.3
A-B	6.6	10.6	12.5	22.8	8.7	15.3	12.5	26.2	15.5
full	17.1	31.3	29.1						

[a]The angle α indicates the maximum deviation of edge C atoms as compared to the reference planar H-GNF, as shown in Figure 2.

at the edges of a graphene ribbon allow modifying the ionization potential (IP) and the electron affinity (EA) of the system with respect to the reference H-passivated flake.[23] The optical characteristics are then directly affected.[26] However, the edge decoration of the flakes induces also structural modifications, which are closely related and interdependent with the electronic stabilization, as we will see in the following.

Figure 2 shows that, depending on the value of N (even or odd), the type of substituent, and the functionalization scheme (A-B or A-A), different types of distortions can arise, either localized at the edges or extended to the flake backbone. For instance, $COCH_3$ represents a typical case where structural modifications are mostly localized at the edges: there is a slight difference for different N and schemes; however, there are no global, coherent modifications. In this case, local steric effects among the functional groups play a primary role in driving distortions: $COCH_3$ groups, which can reorient to minimize the repulsion, induce a relatively small tilt of edge C rings to opposite directions, perpendicular to the flake basal plane (z axis; see Figure 2). As a second example, we highlight the case of the NH_2 termination: here, the interplay of functionalization pattern, group rigidity, and steric effects can produce coherent distortions involving the whole flake backbone, which thus stabilize the structure. This is evident for $N = 7$ ($N = 8$) in the A-A (A-B) scheme (Figure 2), where the system tends to twist along its longitudinal axis (x). For $N = 8$ in the A-A scheme, a "rippling" mode tends also to appear on top of the local distortions induced at the edges.

To quantify these effects, we introduce an angle α, defined as the maximum deviation of edge C atoms with respect to the reference planar configuration (H-GNF, $\alpha = 0$). The values of α for different functional groups are reported in Table 1 for $N = 7$ GNFs (see the Supporting Information for $N = 8$ and $N = 9$, Table S3). In the case of halogen termination, similar distortion angles are observed for both A-A and A-B schemes, while a significantly larger tilting angle is produced upon full functionalization. For molecular substituents, where larger distortions are expected in view of their size, the tilt of edge C rings is considerably reduced when the groups are relatively free to rearrange, as we described for $COCH_3$. This is also the case of methoxy (OCH_3) and $OCF{=}CF_2$ groups, where the flexible O-linkage allows them to assume an ordered alignment (see the Supporting Information, Figure S1). On the contrary, larger α angles (and global distortions) are noticed for rigid groups, such as NH_2 and ethene units ($CH{=}CF_2$ and $CH{=}CH_2$). We remark finally that, even when we find discernible structural modifications, they do not result in any significant local deviation from the regular graphene bonding and no strongly localized defects appear. For further structural details

dx.doi.org/10.1021/jp300657k | J. Phys. Chem. C 2012, 116, 17328−17335

(edge C−C and C-substituent bond lengths), see the Supporting Information, Tables S1 and S2.

We now move to the electronic properties and list in Table 2 the total dipole arising in the presence of different substitution

Table 2. Components of the Dipole Moment for Edge-Functionalized N = 7 GNFs (One Substituent per Class), According to the A-A and A-B Functionalization Schemes

group	scheme	μ_x [D]	μ_y [D]	μ_z [D]
F	A-A	4.848	0.479	0.028
	A-B	−0.001	−0.003	−0.061
NH_2	A-A	−9.335	−0.026	−0.121
	A-B	0.339	−1.238	3.823
$COCH_3$	A-A	9.764	1.138	−0.049
	A-B	0.166	−0.139	0.269

patterns. We notice that a large dipole along the flake longitudinal axis (x) appears for odd N (here, N = 7) in the A-A functionalization scheme, whereas it is almost negligible for the other scheme. The situation is reversed for even N (e.g., N = 8; see the Supporting Information, Table S4). As shown in Table 2 and in Figure 3a, the dipole orientation and intensity depend on the characteristics of the functional group: electron-donating (e.g., NH_2) and electron-withdrawing groups (e.g., F and $COCH_3$) produce large longitudinal dipoles oriented in opposite directions (see also Figure 3a). The presence of a sizable longitudinal dipole (A-A pattern for N = 7 GNF) is accompanied by a spatial localization of the frontier orbitals on opposite sides of the flake. As depicted in Figure 3b, for $\mu_x \neq 0$, the potential well describing the flake assumes a "sawtooth" profile (see, e.g., ref 58), whose height and orientation depend on the magnitude and on the sign of μ_x. Hence, the HOMO and LUMO states present a similar asymmetric character in both cases, but with spatially opposite localization (see Figure 3b). On the other hand, for the A-B scheme, the π distribution of the frontier orbitals undergoes only local modifications, specifically related to the altered symmetry of the flake,[59] as shown in Figure 3c. The modified symmetry of the frontier orbitals is particularly evident for the NH_2 termination, whereas it is less apparent for groups bonded through a C bond, such as $COCH_3$. See the Supporting Information for a more complete analysis of the substituents and family dependence (Figures S1 and S2).

In Table 3, we report the differences of IP and EA (ΔEA and ΔIP) of N = 7 functionalized GNFs with respect to the reference hydrogenated flake, as well as their energy gap (E_G). As expected, an uneven shift of IP and EA is produced upon functionalization, related to the electronegativity of the substituents; for instance, highly electronegative halogen terminations upshift EA more significantly than IP, while strongly electron-donating amino groups downshift IP more than EA. In any case, a gap reduction is always encountered. In the case of C-bonded terminations, a further contribution to the gap reduction is given by the increased effective width of the flake, driven by the extended π-conjugation.

In addition to this well-established behavior, we here more directly estimate the role played by structural distortions. To quantify this effect, we consider model flakes obtained by removing the functionalizing groups from the final structure, and by then H-passivating the remaining dangling bonds: this model structure allows us to decouple the influence of distortions from the overall influence of edge functionalization. By inspecting Table 3, we find a total gap reduction upon functionalization ranging from 200 to 700 meV. The comparison with the values of E_G obtained for the model distorted H-GNFs (in italics in Table 3) points to a non-negligible contribution of structural distortions, corresponding to 35−55% of the total amount. These results are very similar to what is expected for thermal deviations from the ideal structure.[60] It is also worth noting that this trend is mostly independent of the functionalization scheme, with a maximum difference of 80 meV for the NH_2 case, where the two schemes induce significantly different distortion patterns.

Starting from the AM1 results described above, we now turn to the analysis of optical excitations, as obtained from ZINDO calculations. To address the role of both molecular-symmetry and structural modifications, we first consider the N = 7 GNF

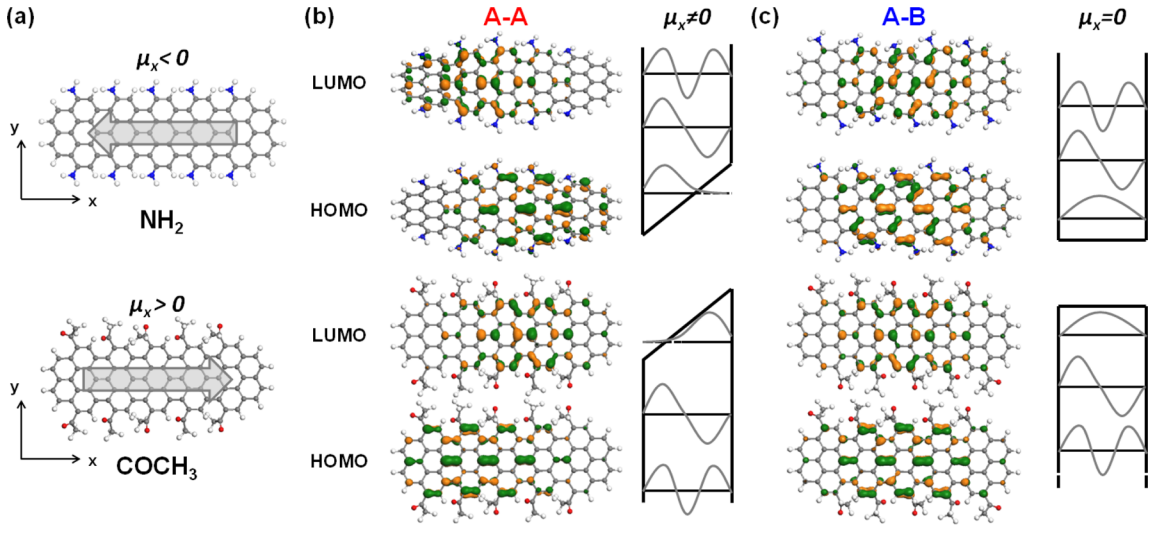

Figure 3. (a) A-A functionalization of N = 7 GNF by means of electron-donating (e.g., NH_2) and electron-withdrawing (e.g., $COCH_3$) groups gives rise to longitudinal dipoles (μ_x) oriented in opposite directions. The frontier orbitals of NH_2- and $COCH_3$-substituted N = 7 GNFs are shown for the (b) A-A and (c) A-B schemes. The square well potential profiles modulating the molecular orbital distribution are sketched in the presence (b) and absence (c) of a longitudinal dipole along the flake.

dx.doi.org/10.1021/jp300657k | J. Phys. Chem. C 2012, 116, 17328−17335

Table 3. Differences of EA and IP (ΔEA and ΔIP, in eV) with Respect to the Reference Hydrogenated (H) Flake and Energy Gap (E_G, in eV) Computed through the AM1 Model for N = 7 GNFs, Functionalized According to the A-B Scheme[a]

		halogens				direct bond				C bond			
		F		Cl	Br	NH_2		OCH_3	$OCF{=}CF_2$	$COCH_3$		$CH{=}CF_2$	$CH{=}CH_2$
	H	A-A	A-B			A-A	A-B			A-A	A-B		
ΔEA	0.00	0.57	0.58	0.53	0.62	−0.18	−0.14	−0.12	0.70	0.74	0.69	0.67	0.14
		0.01	*0.01*			*0.08*	*0.04*			*0.01*	*0.01*		
ΔIP	0.00	0.37	0.32	0.30	0.39	−0.75	−0.79	−0.50	0.31	0.49	0.42	0.19	−0.22
		-0.10	*-0.10*			*-0.24*	*-0.19*			*-0.10*	*-0.10*		
E_G	5.13	4.92	4.87	4.90	4.90	4.55	4.47	4.75	4.74	4.88	4.86	4.65	4.76
		5.01	*5.01*			*4.81*	*4.90*			*5.01*	*5.01*		

[a]For selected groups, we report the values of ΔEA, ΔIP, and E_G also for the A-A scheme and for H-terminated model flakes with the corresponding distorted geometries (in italics).

functionalized with NH_2, where these effects are both prominent. In Figure 4, we report the optical spectra for both

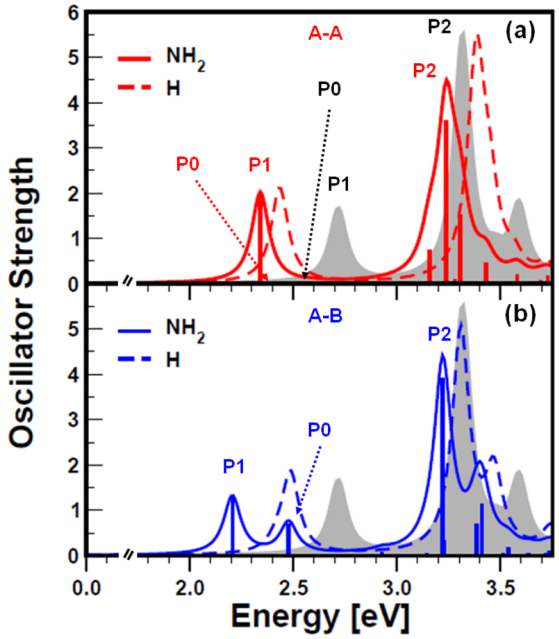

Figure 4. Optical spectra of GNFs with a width parameter of N = 7, functionalized with NH_2 groups, according to the (a) A-A and (b) A-B functionalization schemes. In addition to the spectrum of the planar H-terminated flake taken as a reference (gray shaded area, with the main excitations highlighted in (a)), we show the spectrum of model GNFs obtained by removing the edge substituents from the final structures and H-passivating the dangling bonds (dashed lines), in order to perform a rigorous analysis of distortion effects. All the curves are obtained through a Lorentzian broadening of 50 meV.

functionalization schemes, A-A (red) and A-B (blue), together with the spectrum of the flat H-GNF (gray shaded area), taken as a reference. In addition, we include the spectrum of the H-terminated distorted model flake described above (dashed line), which enables a direct analysis of the distortion effects. As already discussed,[61] the optical spectrum of the planar N = 7 H-GNF shows two main peaks in the low-energy region with longitudinal polarization (along the x axis), labeled as P1 and P2; in addition, a transversally polarized weak excitation (P0) is found at lower energy. Our results indicate that edge functionalization is responsible for a red shift of the P1 peak by 380 and 510 meV in the A-A (Figure 4a) and A-B schemes (Figure 4b), respectively. Remarkably, a further peak is observed in the optical spectrum of the A-B functionalized flake, related to the oscillator strength (OS) increase of P0 by about 3 orders of magnitude. This OS gain is a purely symmetry effect: the molecular symmetry reduction induced by functionalization (from D_{2h} in the H-GNF to C_{2h} in the A-B scheme) implies that the HOMO state acquires the same symmetry as the HOMO-1 one so that the HOMO → LUMO transition is now allowed to contribute to the P0 excitation (see Table 4). This symmetry effect is, in fact, not observed in the A-A functionalized flake.

Table 4. Energy, Oscillator Strength (OS), and Composition in Terms of Molecular Orbital Transitions of the Main Excitations of Functionalized N = 7 GNFs, in the Presence of One Prototypical Substituent per Class, i.e., F, NH_2 (also A-A Scheme), and $COCH_3$, in Addition to the Reference Hydrogenated System[a]

termination	excitation	energy [eV]	OS	transitions (weight)
H	P0	2.54	0.0005	H-1 → L (0.37)
				H → L + 1 (0.39)
	P1	2.72	1.62	H → L (0.79)
	P2	3.32	5.43	H-3 → L + 3 (0.12)
				H-1 → L + 1 (0.76)
F	P0	2.43	0.21	H-1 → L (0.27)
				H → L (0.12)
				H → L + 1 (0.37)
	P1	2.58	1.54	H → L (0.68)
	P2	3.26	5.11	H-3 → L + 3 (0.20)
				H-1 → L + 1 (0.71)
NH_2–A-A	P1	2.34	1.98	H → L (0.75)
	P0	2.35	0.02	H-2 → L (0.29)
				H → L + 1 (0.39)
	P2	3.24	3.59	H-2 → L + 1 (0.50)
NH_2–A-B	P1	2.21	1.29	H → L (0.63)
	P0	2.48	0.70	H-2 → L (0.22)
				H → L (0.18)
				H → L + 1 (0.40)
	P2	3.22	3.92	H-2 → L + 1 (0.53)
				H → L + 1 (0.10)
$COCH_3$	P0	2.42	0.04	H-1 → L (0.34)
				H → L + 1 (0.40)
	P1	2.55	1.68	H → L (0.78)
	P2	3.21	5.13	H-1 → L + 1 (0.71)

[a]In the last column, we report the MO transitions contributing to each excitation, which have a relative weight larger than 0.1.

dx.doi.org/10.1021/jp300657k | J. Phys. Chem. C 2012, 116, 17328−17335

Concerning the role of structural distortion, we observe that the largely distorted geometry produced by the A-A functionalizion (dashed line in Figure 4a) is responsible for about 75% of the optical gap reduction, as noticed by comparing the excitation energy of P1 for the three curves in Figure 4a. P1 is now energetically degenerate with the dark excitation P0, also red shifted about 200 meV with respect to the reference H-GNF (see Table 4). It is worth noting that the frontier orbital localization observed for the A-A scheme in the presence of polar functional groups (see Figure 3b) does not affect the basic features of the main excitations: despite their spatial localization, the overlap between the frontier orbitals is still large enough to preserve the intensity of P1, in comparison with both the reference H-terminated and the A-B functionalized GNF. In the case of the A-B functionalization pattern, distortions contribute to about 45% of the whole optical gap red shift: the impact of distortions is less pronounced for this structure, and molecular symmetry effects dominate (see Figure 4b).

We next inspect the role of the chemical specificities of edge substituents, by comparing the optical spectra of $N = 7$ GNFs functionalized with all the anchoring groups considered in this work, as shown in Figure 5. We here consider only the A-B pattern, since negligible differences are observed between the two schemes for most of the substituents (see Figure S3 in the Supporting Information for more details). The analysis of fully halogen-terminated GNFs is also included in the Supporting Information (see Figure S4 and Table S8). A nonrigid red shift of the spectra is generally observed upon functionalization, with a larger red shift for P1 than for P2. All the spectra of the GNFs functionalized with groups anchored through a direct bond (Figure 5b) display the same key feature already discussed for the amino termination and reported in Figure 4b: an additional distinct peak emerges, corresponding to the P0 excitation, which becomes optically active. This effect is also present, even though less intense, for halogen terminations: P0 appears as a shoulder in the main P1 peak for fluorinated flakes (Figure 5a). In the case of C-bonded molecular substituents, the impact of functionalization on the electronic states is further reduced so that the main spectral features are basically preserved with respect to the flat H-terminated flake (see spectra in Figure 5b and the composition of the main excitations in Table 4).

To complete our analysis, we finally investigate the spectra of the GNFs with width parameters $N = 8$ and $N = 9$, functionalized with one prototypical group per class, namely, F, NH_2, and $COCH_3$, according to the higher-symmetry scheme (A-A for $N = 8$ and A-B for $N = 9$). The optical spectra computed for these systems are shown in Figure 6, with the reference spectrum of the corresponding planar H-GNF

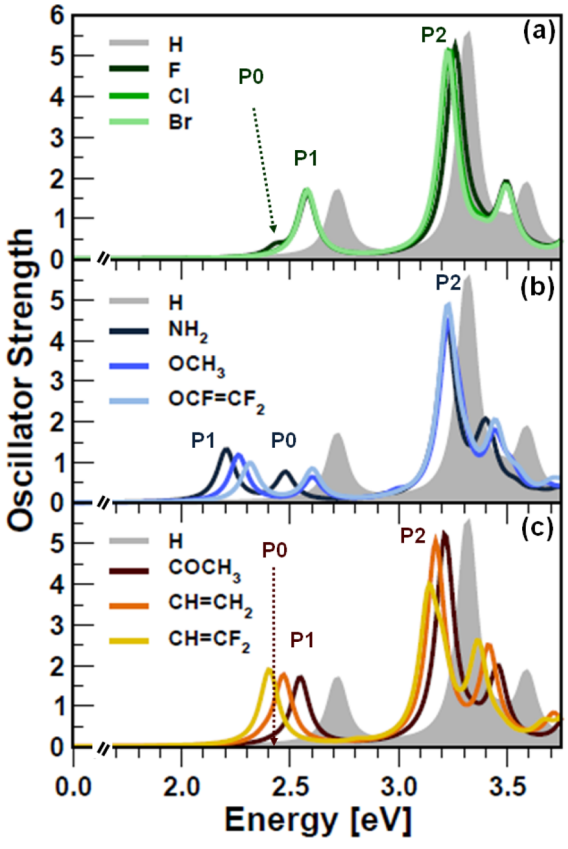

Figure 5. Optical spectra $N = 7$ GNFs functionalized in the A-B scheme with each termination considered in this work, including (a) halogen atoms, (b) directly- and (c) C-bonded groups. In each panel, we indicate for one of the groups the three main excitations described in the text, i.e., P0, P1, and P2. Moreover, the spectrum of the reference H-flake is reported (gray shaded area in each panel). All the curves are obtained through a Lorentzian broadening of 50 meV.

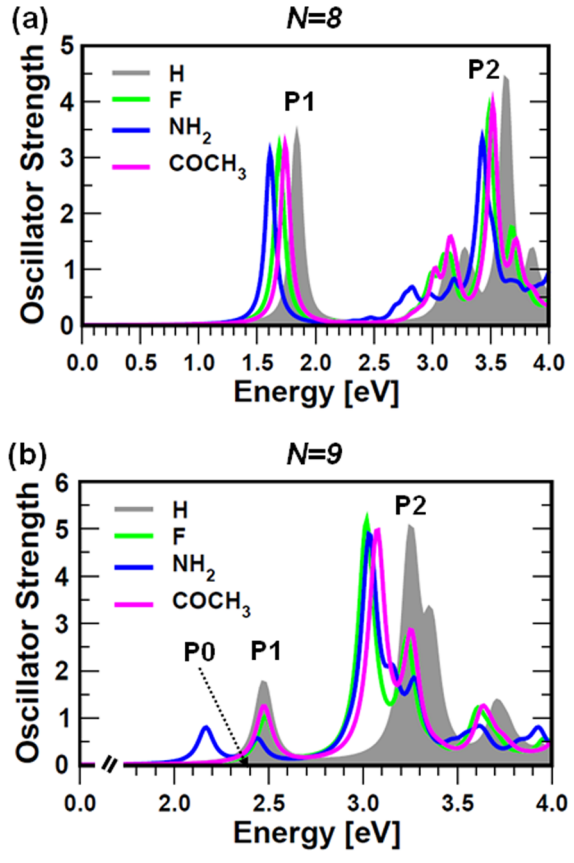

Figure 6. Optical spectra of symmetrically functionalized GNFs with width parameters (a) $N = 8$ (A-A scheme) and (b) $N = 9$ (A-B scheme). One edge substituent for each class of terminations considered in this work is addressed for both GNFs. The spectrum of the reference H-GNF is reported in the background of each panel (gray shaded area) with the indication of the main excitations (P0, P1, and P2). All the curves are obtained through a Lorentzian broadening of 50 meV.

dx.doi.org/10.1021/jp300657k | J. Phys. Chem. C 2012, 116, 17328−17335

reported in the background of each panel (gray shaded area). The optical spectrum of the $N = 8$ GNF is dominated by a first intense peak P1, which is about 1 eV lower in energy compared with those of the other GNF families (compare Figure 6a with Figures 5 and 6b), in agreement with the trend for the electronic gaps.[23] Contrary to $N = 7$, this peak always corresponds to the lowest-energy excitation, regardless of the edge termination (see the Supporting Information, Table S5). Moreover, we do not observe any functionalization-induced modification in the π distribution of frontier orbitals, since the molecular symmetry remains the same in the A-A scheme (C_{2h}). In this case, the main effect of functionalization is thus to red shift the spectrum with respect to the reference H-GNF, in an almost rigid fashion (up to over 200 meV upon amino termination).

On the other hand, the optical spectra of $N = 9$ GNFs manifest more similarities with those of $N = 7$ GNFs (see Figures 6b and 5 for comparison), both in the spectral shape and in the composition of the main excitations (see the Supporting Information, Table S6). Also for the ribbons belonging to the $N = 3p$ family, the P0 excitations become optically active, giving rise to a distinct peak in the presence of NH_2 functional groups, according to the mechanism described for the $N = 7$ GNFs. The lowest-energy peak is red shifted by about 300 meV upon amino substitution, compared to the reference H-GNF. In the presence of other edge substituents (F and $COCH_3$), the energy of P1 is basically unaffected, while P2 is red shifted about 200 meV upon each termination (see Figure 6b). This is an effect of the MO distribution observed for the GNFs belonging to this family, for which the frontier orbitals present a reversed orientation of the π distribution with respect to the flakes of the $N = 3p + 1$ family (see Figure S2, Supporting Information).

CONCLUSIONS

We have analyzed in detail the effects of edge covalent functionalization on the structural, electronic, and optical properties of armchair graphene nanoflakes. Different functionalization groups and patterns have been discussed for a specific flake, and the analysis has been extended and rationalized for additional systems, according to the armchair width modulation. Our results indicate that the steric repulsion among substituents generally determines local distortions at the edges, even though structural modifications can involve the whole flake backbone in specific cases. Functionalization-induced distortions are found to play an effective role in the electronic gap reduction experienced by the flakes, with contributions ranging from 35% to 55% of the total gap decrease. Depending on the functionalization pattern and the character of the substituents, insteresting charge-redistribution effects are seen for the frontier orbitals, related to either the modified molecular symmetry or the appearance of a large longitudinal dipole component. All of these effects are reflected in the optical spectra: distortions largely contribute to the lowering of the optical gap (up to 300 meV), while the appearance of an additional peak at low energy is related to the distribution and the characteristics of the functional groups. Our results indicate that the interplay among the system symmetry, the chemical features, and the distribution of the substituents, as well as the resulting structural distortions, is crucial to understanding the modification of the optoelectronic properties of functionalized graphene nanoflakes.

ASSOCIATED CONTENT

Supporting Information

The Supporting Information is organized into three sections. In the first one, we report the structural details (bond lengths and distortion angles) of the optimized $N = 7$, $N = 8$, and $N = 9$ graphene nanoflakes to complete the data reported in the main text. The second section supports the analysis of the electronic properties, including a table with the dipole moment components of $N = 8$ and $N = 9$ GNFs (functionalized according to both A-A and A-B schemes) and the isosurfaces of the frontier orbitals for the considered systems. The last part is dedicated to optical properties. The analysis of the effects related to different functionalization schemes and structural distortions are extended here also to $COCH_3$ and F terminations, as representatives of the classes of C-bonded and halogen substituents. We also include the tables with the composition of the main excitations for $N = 8$ and $N = 9$ GNFs, and the analysis of the optical features of full halogen-terminated GNFs (only $N = 7$). This material is available free of charge via the Internet at http://pubs.acs.org.

AUTHOR INFORMATION

Corresponding Author

*E-mail: caterina.cocchi@unimore.it (C.C.), deborah.prezzi@unimore.it (D.P.).

Notes

The authors declare no competing financial interest.

ACKNOWLEDGMENTS

The authors are grateful to Stefano Corni for fruitful discussions and acknowledge CINECA for computational support. This work was partly supported by the Italian Ministry of University and Research under FIRB grant ItalNanoNet, and by Fondazione Cassa di Risparmio di Modena with project COLDandFEW. M.J.C. acknowledges support from FAPESP and CNPq (Brazil).

REFERENCES

(1) Castro Neto, A. H.; Guinea, F.; Peres, N. M. R.; Novoselov, K. S.; Geim, A. K. *Rev. Mod. Phys.* **2009**, *81*, 109−162.
(2) Nakada, K.; Fujita, M.; Dresselhaus, G.; Dresselhaus, M. S. *Phys. Rev. B* **1996**, *54*, 17954−17961.
(3) Son, Y.-W.; Cohen, M. L.; Louie, S. G. *Phys. Rev. Lett.* **2006**, *97*, 216803.
(4) Barone, V.; Hod, O.; Scuseria, G. E. *Nano Lett.* **2006**, *6*, 2748−2754.
(5) Prezzi, D.; Varsano, D.; Ruini, A.; Marini, A.; Molinari, E. *Phys. Rev. B* **2008**, *77*, 041404(R).
(6) Yang, L.; Cohen, M.; Louie, S. *Nano Lett.* **2007**, *7*, 3112−3115.
(7) Yang, L.; Cohen, M. L.; Louie, S. G. *Phys. Rev. Lett.* **2008**, *101*, 186401.
(8) Yazyev, O. *Rep. Prog. Phys.* **2010**, *73*, 056501.
(9) Pisani, L.; Chan, J. A.; Montanari, B.; Harrison, N. M. *Phys. Rev. B* **2007**, *75*, 064418.
(10) Son, Y.-W.; Cohen, M. L.; Louie, S. G. *Nature (London)* **2006**, *444*, 347−349.
(11) Hod, O.; Barone, V.; Peralta, J. E.; Scuseria, G. E. *Nano Lett.* **2007**, *7*, 2295−2299.
(12) Gunlycke, D.; Li, J.; Mintmire, J. W.; White, C. T. *Appl. Phys. Lett.* **2007**, *91*, 112108.
(13) Kan, E.-j.; Li, Z.; Yang, J.; Hou, J. G. *J. Am. Chem. Soc.* **2008**, *130*, 4224−4225.
(14) Wu, M.; Wu, X.; Zeng, X. *J. Phys. Chem. C* **2010**, *114*, 3937−3944.

(15) Rigo, V.; Martins, T.; da Silva, A.; Fazzio, A.; Miwa, R. *Phys. Rev. B* **2009**, *79*, 075435.
(16) Longo, R. C.; Carrete, J.; Ferrer, J.; Gallego, L. J. *Phys. Rev. B* **2010**, *81*, 115418.
(17) Wang, Y.; Cao, C.; Cheng, H. *Phys. Rev. B* **2010**, *82*, 205429.
(18) Cocchi, C.; Prezzi, D.; Calzolari, A.; Molinari, E. *J. Chem. Phys.* **2010**, *133*, 124703.
(19) Cervantes-Sodi, F.; Csányi, G.; Piscanec, S.; Ferrari, A. C. *Phys. Rev. B* **2008**, *77*, 165427.
(20) Ren, H.; Li, Q.; Su, H.; Shi, Q. W.; Chen, J.; Yang, J. eprint **2007**, arXiv0711.1700v1 *[cond-mat.mtrl-sci]*.
(21) Lu, Y.; Wu, R.; Shen, L.; Yang, M.; Sha, Z.; Cai, Y.; He, P.; Feng, Y. *Appl. Phys. Lett.* **2009**, *94*, 122111.
(22) Wang, W.; Li, Z. *J. Appl. Phys.* **2011**, *109*, 114308.
(23) Cocchi, C.; Ruini, A.; Prezzi, D.; Caldas, M. J.; Molinari, E. *J. Phys. Chem. C* **2011**, *115*, 2969−2973.
(24) Zhu, X.; Su, H. *J. Phys. Chem. C* **2010**, *114*, 17257−17262.
(25) Prezzi, D.; Varsano, D.; Ruini, A.; Molinari, E. *Phys. Rev. B* **2011**, *84*, 041401.
(26) Cocchi, C.; Prezzi, D.; Ruini, A.; Caldas, M.; Molinari, E. *J. Phys. Chem. Lett.* **2011**, *2*, 1315−1319.
(27) Wagner, P.; Ewels, C. P.; Ivanovskaya, V. V.; Briddon, P. R.; Pateau, A.; Humbert, B. *Phys. Rev. B* **2011**, *84*, 134110.
(28) Rosenkranz, N.; Till, C.; Thomsen, C.; Maultzsch, J. *Phys. Rev. B* **2011**, *84*, 195438.
(29) Bets, K.; Yakobson, B. *Nano Res.* **2009**, *2*, 161−166.
(30) Shenoy, V. B.; Reddy, C. D.; Zhang, Y.-W. *ACS Nano* **2010**, *4*, 4840−4844.
(31) Lu, Q.; Huang, R. *Phys. Rev. B* **2010**, *81*, 155410.
(32) Peng, X.; Velasquez, S. *Appl. Phys. Lett.* **2011**, *98*, 023112.
(33) Sadrzadeh, A.; Hua, M.; Yakobson, B. *Appl. Phys. Lett.* **2011**, *99*, 013102.
(34) Wu, J.; Pisula, W.; Muellen, K. *Chem. Rev.* **2007**, *107*, 718−747.
(35) Kosynkin, D. V.; Higginbotham, A. L.; Sinitskii, A.; Lomeda, J. R.; Dimiev, A.; Price, B. K.; Tour, J. M. *Nature (London)* **2009**, *458*, 872.
(36) Jiao, L.; Zhang, L.; Wang, X.; Diankov, G.; Dai, H. *Nature (London)* **2009**, *458*, 877.
(37) Cai, J.; Ruffieux, P.; Jaafar, R.; Bieri, M.; Braun, T.; Blankenburg, S.; Muoth, M.; Seitsonen, A. P.; Saleh, M.; Feng, X.; Müllen, K.; Fasel, R. *Nature (London)* **2010**, *466*, 470−473.
(38) Jia, X.; Campos-Delgado, J.; Terrones, M.; Meunier, V.; Dresselhaus, M. *Nanoscale* **2010**, *3*, 86−95.
(39) Palma, C.; Samorí, P. *Nat. Chem.* **2011**, *3*, 431−436.
(40) Blankenburg, S.; Cai, J.; Ruffieux, P.; Jaafar, R.; Passerone, D.; Feng, X.; Müllen, K.; Fasel, R.; Pignedoli, C. A. *ACS Nano* **2012**, *6*, 2020−2025.
(41) AM1 and ZINDO/S calculations were performed using the VAMP package included in the Accelrys Materials Studio software, version 5.0 (http://accelrys.com/products/materials-studio).
(42) Wetmore, S. D.; Boyd, R. J.; Eriksson, L. A. *Chem. Phys. Lett.* **2000**, *322*, 129−135.
(43) Caldas, M. J.; Pettenati, E.; Goldoni, G.; Molinari, E. *Appl. Phys. Lett.* **2001**, *79*, 2505−2507.
(44) Dávila, L. Y. A.; Caldas, M. J. *J. Comput. Chem.* **2002**, *23*, 1135.
(45) Kubatkin, S.; Danilov, A.; Hjort, M.; Cornil, J.; Brédas, J.; Stuhr-Hansen, N.; Hedegård, P.; Bjørnholm, T. *Nature (London)* **2002**, *32*, 567−569.
(46) Dewar, M. J. S.; Zoebish, E. G.; Healy, E. F.; Stewart, J. J. P. *J. Am. Chem. Soc.* **1985**, *107*, 3902−3909.
(47) Ridley, J.; Zerner, M. *Theor. Chim. Acta* **1973**, *32*, 111−134.
(48) Shemella, P.; Zhang, Y.; Mailman, M.; Ajayan, P.; Nayak, S. *Appl. Phys. Lett.* **2007**, *91*, 042101.
(49) Hod, O.; Barone, V.; Scuseria, G. E. *Phys. Rev. B* **2008**, *77*, 035411.
(50) Bader, R.; Chang, C. *J. Phys. Chem.* **1989**, *93*, 2946−2956.
(51) Hehre, W.; Radom, L.; Pople, J. *J. Am. Chem. Soc.* **1972**, *94*, 1496−1504.
(52) Zhang, Q.; Prins, P.; Jones, S. C.; Barlow, S.; Kondo, T.; An, Z.; Siebbeles, L. D. A.; Marder, S. R. *Org. Lett.* **2005**, *7*, 5019−5022.
(53) Kikuzawa, Y.; Mori, T.; Takeuchi, H. *Org. Lett.* **2007**, *9*, 4817−4820.
(54) Wang, X.; Li, X.; Zhang, L.; Yoon, Y.; Weber, P. K.; Wang, H.; Guo, J.; Dai, H. *Science* **2009**, *324*, 768−771.
(55) Bock, C. W.; Trachtman, M.; George, P. *J. Mol. Struct.:THEOCHEM* **1985**, *122*, 155−172.
(56) Campanelli, A. R.; Domenicano, A.; Ramondo, F. *J. Phys. Chem. A* **2003**, *107*, 6429−6440.
(57) Krygowski, T.; Stepien, B. *Chem. Rev.* **2005**, *105*, 3482−3512.
(58) Rissner, F.; Egger, D. A.; Natan, A.; Körzdörfer, T.; Kümmel, S.; Kronik, L.; Zojer, E. *J. Am. Chem. Soc.* **2011**, *133*, 18634−18645.
(59) The HOMO (LUMO) level of the $N = 7$ H-terminated flake (D_{2h} point group) has B_{3u} (B_{2g}) symmetry. Within the A-B functionalization scheme, the flake symmetry reduces to C_{2h} and, consequently, the HOMO (LUMO) becomes an A_u (B_g) state. It is worth recalling that the symmetry considerations reported here are for ideal unrelaxed systems. Structural optimization further lowers the symmetry of functionalized flakes and, consequently, locally affects also the molecular orbital distribution.
(60) Martin-Samos, L.; Bussi, G.; Ruini, A.; Molinari, E.; Caldas, M. J. *Phys. Rev. B* **2010**, *81*, 081202.
(61) Cocchi, C.; Prezzi, D.; Ruini, A.; Benassi, E.; Caldas, M. J.; Corni, S.; Molinari, E. *J. Phys. Chem. Lett.* **2012**, *3*, 924−929.